Spin-flavor precession of Dirac neutrinos in dense matter and its potential in core-collapse supernovae

Hirokazu Sasaki[®], ^{1,*} Tomoya Takiwaki[®], ² and A. Baha Balantekin[®]

¹Los Alamos National Laboratory, Los Alamos, New Mexico 87545, USA

²National Astronomical Observatory of Japan, 2-21-1 Osawa, Mitaka, Tokyo 181-8588, Japan

³Department of Physics, University of Wisconsin, Madison, Wisconsin 53706, USA

(Received 14 September 2023; accepted 27 October 2023; published 29 November 2023)

We calculate the spin-flavor precession (SFP) of Dirac neutrinos induced by strong magnetic fields and finite neutrino magnetic moments in dense matter. As found in the case of Majorana neutrinos, the SFP of Dirac neutrinos is enhanced by the large magnetic field potential and suppressed by large matter potentials composed of the baryon density and the electron fraction. The SFP is possible irrespective of the large baryon density when the electron fraction is close to 1/3. The diagonal neutrino magnetic moments that are prohibited for Majorana neutrinos enable the spin precession of Dirac neutrinos without any flavor mixing. With supernova hydrodynamics simulation data, we discuss the possibility of the SFP of both Dirac and Majorana neutrinos in core-collapse supernovae. The SFP of Dirac neutrinos occurs at a radius where the electron fraction is 1/3. The required magnetic field of the proto-neutron star for the SFP is a few 10¹⁴ G at any explosion time. For the Majorana neutrinos, the required magnetic field fluctuates from 10¹³ G to 10¹⁵ G. Such a fluctuation of the magnetic field is more sensitive to the numerical scheme of the neutrino transport in the supernova simulation.

DOI: 10.1103/PhysRevD.108.103046

I. INTRODUCTION

Dirac versus Majorana nature remains one of the biggest questions in neutrino physics. During the last several decades, numerous experimental and theoretical efforts were made to answer this question [1]. Neutrinoless double beta $(0\nu\beta\beta)$ decay is a promising probe into Majorana neutrinos, and lower limits for the decay half-life on various nuclei were continuously updated by many experiments [2]. The usual neutrino oscillation experiments cannot distinguish between Dirac and Majorana neutrinos because the flavor conversions in vacuum and matter are associated with the differences of the squares of neutrino masses not the individual masses. These experiments are not sensitive to the Majorana phases either [3]. On the other hand, the coupling of the stellar magnetic field and finite neutrino magnetic moments potentially induces the spin-flavor precession (SFP) between left-handed and right-handed neutrinos in astrophysical sites [4-6]. Such a SFP is completely different from the usual flavor conversions

Published by the American Physical Society under the terms of the Creative Commons Attribution 4.0 International license. Further distribution of this work must maintain attribution to the author(s) and the published article's title, journal citation, and DOI. Funded by SCOAP³. conserving the neutrino chirality, and its properties are sensitive to Dirac versus Majorana nature.

Recent experiments (e.g., XENONnT [7], CONUS [8], Dresden-II reactor and COHERENT [9], and XMASS-I [10]) constrained the value of the neutrino magnetic moment. Among them, the XENONnT experiment gives the most stringent upper limit, $\mu_{\nu} < 6.4 \times 10^{-12} \mu_{B}$ (90% C.L.) [7], where μ_{B} is the Bohr magneton. In addition to the terrestrial experiments, the value of the neutrino magnetic moment can be constrained from the thermal evolution of astronomical phenomena [11–15]. Currently, neutrino energy loss in globular clusters imposes on the most stringent value, $\mu_{\nu} < 1.2 \times 10^{-12} \mu_{B}$ [12].

A strong magnetic field larger than 10¹² G is possible in explosive astrophysical sites such as core-collapse supernovae and neutron star mergers (see [16–28] and the references therein). Large numbers of neutrinos produced there potentially contain information about the magnetic field effects on neutrino oscillations. We note that the neutrino flux from astrophysical sites can be affected by even small intergalactic and interstellar magnetic fields (nG–uG) [29,30].

Currently, operational neutrino observatories can detect of the order of 10⁴ neutrino events from a core-collapse supernova in the Galaxy [31]. Such high statistical neutrino signals enable the investigation of neutrino oscillations inside the star [32–35]. Furthermore, the nucleosynthesis of heavy nuclei induced by neutrino absorption, such as the

hsasaki@lanl.gov

 νp process [36–39] and the ν process [40–42], is sensitive to large neutrino fluxes near the proto-neutron star (PNS). Therefore, observable quantities such as solar abundances and elemental abundances of heavy nuclei leave clues to the supernova neutrino [38,39].

It is predicted that neutrino oscillations in core-collapse supernovae are affected by the coherent forward scatterings of neutrinos with background matter and neutrinos themselves [43]. Charged current interactions of neutrinos with background electrons induce the Mikheyev-Smirnov-Wolfenstein (MSW) matter effect [44,45]. The neutrinoneutrino interactions cause a nonlinear potential in the neutrino Hamiltonian [46–55] and give various properties of neutrino many-body systems that are vigorously investigated, such as the neutrino fast flavor instability [56] and the many-body nature of collective neutrino oscillations beyond the mean field [57,58].

The SFP is affected by these potentials in core-collapse supernovae. The resonant spin-flavor (RSF) conversion occurs resonantly like the MSW effect at the resonance density in core-collapse supernovae [4,59–71]. Near the PNS, the neutrino-neutrino interactions are no longer negligible, and they contribute to neutrino-antineutrino oscillations of Majorana neutrinos [72–75]. Majorana neutrinos can reach flavor equilibrium in the short scale determined by the strength of the magnetic field potential [74,75]. Such an

equilibration phenomenon is induced by the coupling of matter potentials with the magnetic field potential and is sensitive to the values of both the baryon density and the electron fraction of the supernova material. The neutrino–antineutrino oscillations can occur even with high baryon density if the electron fraction is close to 0.5 [75]. In our previous study (hereafter, Ref. [75] is denoted as ST21), we only focused on the equilibration of Majorana neutrinos. However, the SFP should also be possible for Dirac neutrinos.

In this paper, we study the SFP of Dirac neutrinos in dense matter following a similar framework for Majorana neutrinos in ST21 [75]. We reveal the mechanism of equilibration of Dirac neutrinos and derive a necessary condition for the SFP in dense matter. Then, we investigate the possibility of SFP of both Dirac and Majorana neutrinos in core-collapse supernovae and discuss the difference between both types of neutrinos.

II. METHODS

Figure 1 gives an overview of standard neutrino flavor oscillations as well as the SFP. In the absence of a magnetic field or a neutrino magnetic moment ($\mu_{\nu}B=0$), there is no spin precession among the left- and right-handed neutrinos, and the only separate flavor conversions occur in the

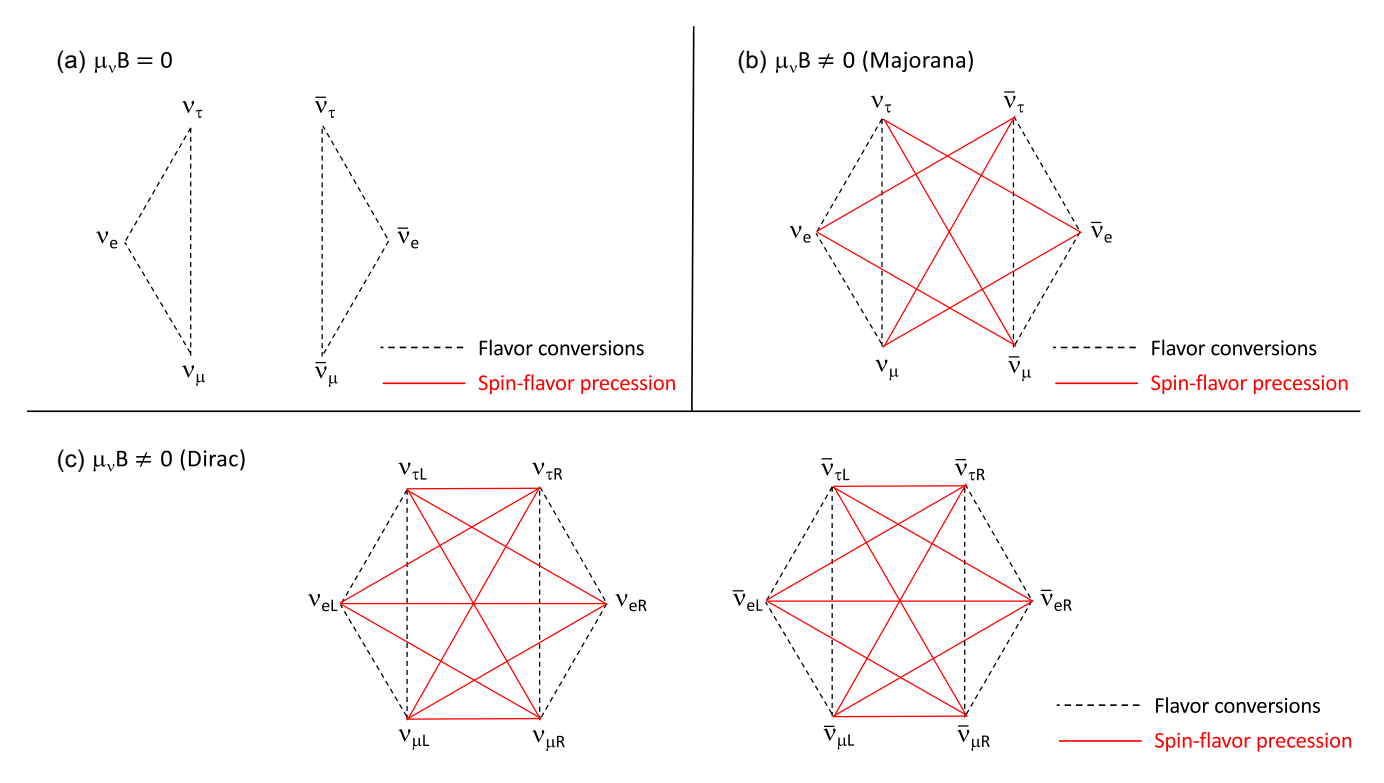


FIG. 1. Overview of the magnetic field effect on neutrino oscillations. (a) Case without the magnetic field effect. The dashed black line shows ordinary flavor conversions in both the neutrino and antineutrino sectors. (b) Case with the magnetic field effect on Majorana neutrinos. The solid red line shows the SFP induced by the finite neutrino magnetic moment and the magnetic field. (c) Magnetic field effect on Dirac neutrinos. The neutrinos and antineutrinos are decoupled from each other. Here, $\nu_{\alpha L}$ and $\bar{\nu}_{\alpha R}(\alpha=e,\mu,\tau)$ correspond to active left-handed neutrinos (ν_{α}) and right-handed antineutrinos ($\bar{\nu}_{\alpha}$) in (a) and (b).

neutrino and the antineutrino sectors, as illustrated in Fig. 1(a). When both the neutrino magnetic moment and the magnetic field are finite $(\mu_{\nu}B \neq 0)$, the SFP occurs together with the usual flavor conversions. For the Majorana neutrinos in Fig. 1(b), the right-handed neutrino corresponds to the antineutrino, and the SFP converts neutrinos into antineutrinos and vice versa. The spin precession without changing the flavor, such as $\nu_{\alpha} \leftrightarrow \bar{\nu}_{\alpha} (\alpha = e, \mu, \tau)$, is prohibited due to the vanishing diagonal magnetic moments for Majorana neutrinos. With a strong magnetic field, Majorana neutrinos can reach an equilibrium of neutrinoantineutrino oscillations [74,75]. On the other hand, for the Dirac neutrinos, the neutrino and antineutrino sectors are decoupled as in Fig. 1(c), and the spin precession, such as $\nu_{\alpha L} \leftrightarrow \nu_{\alpha R}$, is allowed due to the existence of diagonal magnetic moments. The magnetic field effect on neutrino oscillations is significantly different for Majorana and Dirac neutrinos, although there is no difference in ordinary flavor conversions.

We study the magnetic field effect on Dirac neutrino oscillations as in Fig. 1(c), following our previous work on Majorana neutrino oscillations (ST21 [75]). We focus only on conversions of left-handed and right-handed neutrinos and ignore the effect of neutrino-neutrino interactions. We employ the same neutrino emission model as used in ST21 [75], which facilitates the comparison of Dirac and Majorana neutrino oscillations. We consider a single neutrino energy, E=1 MeV, with an emission angle $\theta \in [-\frac{\pi}{3}, \frac{\pi}{3}]$ at a radius r. (This projection angle θ should not be confused with the neutrino mixing angles which carry indices, i.e., θ_{12} .) The neutrino conversions are calculated with the Liouville–von Neumann equation [74,75],

$$\cos\theta \frac{\partial}{\partial r}D = -i[H, D],\tag{1}$$

where D and H are the neutrino density matrix and Hamiltonian for ν_L and ν_R ,

$$D = \begin{pmatrix} \rho_{L\theta} & X_{\theta} \\ X_{\theta}^{\dagger} & \rho_{R\theta} \end{pmatrix}, \tag{2}$$

$$H = \begin{pmatrix} H_L & V_{\text{mag}} \\ V_{\text{mag}}^{\dagger} & H_R \end{pmatrix}, \tag{3}$$

$$H_L = \Omega(E) + V_{\text{mat}}, \tag{4}$$

where $\rho_{L\theta}$ and $\rho_{R\theta}$ are 3×3 density matrices of left- and right-handed neutrinos emitted with the angle θ , and X_{θ} is a correlation between ν_L and ν_R . We use the vacuum term of left-handed neutrinos $\Omega(E)$ in Eq. (8) of Ref. [37] with neutrino mixing parameters, $\{\Delta m_{21}^2, \Delta m_{32}^2, \theta_{12}, \theta_{13}, \theta_{23}\}$, where we assume normal neutrino mass hierarchy $(\Delta m_{32}^2 > 0)$ and no CP phase $(\delta_{CP} = 0)$. The Hamiltonian of the right-handed neutrinos is given by [4]

$$H_R = \frac{\Delta m_{21}^2}{6E} \begin{pmatrix} -2 & 0 & 0\\ 0 & 1 & 0\\ 0 & 0 & 1 \end{pmatrix} + \frac{\Delta m_{32}^2}{6E} \begin{pmatrix} -1 & 0 & 0\\ 0 & -1 & 0\\ 0 & 0 & 2 \end{pmatrix}, \tag{5}$$

where we ignore neutrino mixings and any interaction of the right-handed neutrinos with background particles. The matter potential in Eq. (4) is described by ST21 [75],

$$V_{\text{mat}} = -\frac{\lambda_n}{2} I_{3\times 3} + \lambda_e \begin{pmatrix} 1 & 0 & 0 \\ 0 & 0 & 0 \\ 0 & 0 & 0 \end{pmatrix}, \tag{6}$$

$$\lambda_e = \sqrt{2}G_F \rho_b N_A Y_e, \tag{7}$$

$$\lambda_n = \sqrt{2}G_F \rho_b N_A (1 - Y_e), \tag{8}$$

where G_F is the Fermi coupling constant, ρ_b is the baryon density, N_A is the Avogadro number, Y_e is the electron fraction, and $I_{3\times3}$ is the 3×3 identity matrix. In Eq. (3), $V_{\rm mag}$ is the potential associated with the coupling of neutrino magnetic moments with the magnetic field,

$$V_{\text{mag}} = B_T \begin{pmatrix} \mu_{ee} & \mu_{e\mu} & \mu_{e\tau} \\ \mu_{\mu e} & \mu_{\mu\mu} & \mu_{\mu\tau} \\ \mu_{\tau e} & \mu_{\tau\mu} & \mu_{\tau\tau} \end{pmatrix}, \tag{9}$$

where B_T is a transverse magnetic field perpendicular to the direction of neutrino emission and $\mu_{\alpha\beta}(\alpha,\beta=e,\mu,\tau)$ are neutrino magnetic moments. This magnetic field potential is in the nondiagonal component of Eq. (3), inducing the mixing between left- and right-handed neutrinos. The diagonal neutrino magnetic moments $\mu_{\alpha\alpha}(\alpha=e,\mu,\tau)$ that are ignored in Majorana neutrinos need to be considered in Dirac neutrinos. Here, we assume flavor-independent diagonal terms and antisymmetric nondiagonal terms in Eq. (9),

$$V_{\text{mag}} = \Omega_{\text{d}} I_{3\times 3} + \Omega_{\text{nd}} \begin{pmatrix} 0 & 1 & 1 \\ -1 & 0 & 1 \\ -1 & -1 & 0 \end{pmatrix}, \quad (10)$$

where Ω_d and Ω_{nd} characterize the strengths of diagonal and nondiagonal neutrino magnetic moments.

III. RESULTS AND DISCUSSIONS

We discuss the effect of $\Omega_{\rm nd}$ in Eq. (10) as done in Majorana neutrinos in ST21 [75]. On the other hand, $\Omega_{\rm d}$ terms can induce the SFP without changing the neutrino flavors [e.g., $\nu_{eL} \leftrightarrow \nu_{eR}$ in Fig. 1(c)], which is prohibited for Majorana neutrinos. The SFP of $\Omega_{\rm d}$ terms is different from that of $\Omega_{\rm nd}$. Therefore, we discuss separately the roles of both terms in Secs. III A and III B. Then, we investigate

the possibility of SFP of both Dirac and Majorana neutrinos in core-collapse supernovae in Sec. III C.

A. Nondiagonal magnetic field potential Ω_{nd}

We calculate the magnetic field effect on Dirac neutrino oscillations by setting the initial condition of the diagonal terms of left-handed neutrinos, $(\rho_{L\theta})_{\alpha\alpha} = n_{\nu_\alpha}/n_\nu(\alpha=e,\mu,\tau)$, where $n_\nu = \sum_{\alpha=e,\mu,\tau} n_{\nu_\alpha}$ and $n_{\nu_x}/n_{\nu_e} = 0.4(x=\mu,\tau)$. All of the other components in Eq. (2) are set to zero at r=0. In Sec. III A, we fix the strength of the nondiagonal magnetic field potential $\Omega_{\rm nd} = (\mu_\nu/10^{-12}\mu_B)$ $(B_T/3.4\times10^{14}~{\rm G}) = 0.1~{\rm cm}^{-1}$ and ignore the diagonal term $(\Omega_{\rm d}=0~{\rm cm}^{-1})$. In order to study the sensitivity of the matter potential in Eq. (6), we change the values of the electron fraction Y_e and the baryon density given by $\rho_{\rm b}=5.2\times10^6~{\rm g/cm}^3(Y_e/0.5)^{-1}(\lambda_e/10^{-2}~{\rm cm}^{-1})$.

1. Low density case

Figure 2 shows the result of neutrino number ratios in the fixed values of $\rho_{\rm b}=5.2\times 10^6~{\rm g/cm^3}$ and $Y_e=0.5$, which corresponds to $\lambda_e=0.1\Omega_{\rm nd}$. Such ratios of Dirac neutrinos $\nu_{\alpha s}(\alpha=e,x,y,s=L,R)$ are obtained by averaging the diagonal components of neutrino density matrices,

$$f_{\nu_{as}} = \frac{3}{2\pi} \int_{\frac{\pi}{3}}^{\frac{\pi}{3}} d\theta (\rho_{s\theta})_{\alpha\alpha}, \tag{11}$$

where ν_{xs} and ν_{ys} are eigenstates in a rotated frame described by a linear combination of flavors μ and τ [76]. The magnetic field potential is a dominant term in neutrino Hamiltonians, and SFPs in both the $\nu_{eL} - \nu_{xL} - \nu_{yR}$ and $\nu_{eR} - \nu_{xR} - \nu_{yL}$ sectors are prominent. The vacuum frequencies associated with Δm_{21}^2 and Δm_{32}^2 are negligible compared with $\Omega_{\rm nd}$. Therefore, the values of $f_{\nu_{eL}} + f_{\nu_{xL}} + f_{\nu_{yR}}$ and $f_{\nu_{eR}} + f_{\nu_{xR}} + f_{\nu_{yL}}$ are almost constant. The neutrino ratios are oscillating around the dashed lines, and such equilibrium values are derived in Appendix A 1.

The SFP discussed in Figs. 2–5 is almost independent of the vacuum term and the neutrino mass hierarchy. We remark that the vacuum frequencies can contribute to the SFP, and the hierarchy dependence becomes prominent when the magnetic field potential is comparable with the vacuum frequencies and other potentials in the Hamiltonian are negligible. We mention such a hierarchy difference in core-collapse supernovae in Sec. III C.

2. High density case

Figure 3 shows the result for the case of $\lambda_e=10^2\Omega_{\rm nd}$ with $\rho_{\rm b}=5.2\times10^9~{\rm g/cm^3}$ and $Y_e=0.5$. The numerical setup for Fig. 3 is the same as that of Fig. 2 except for the value of ρ_b . All of the calculated neutrino number ratios are constant $(f_{\nu_{eL}}=5/9,~f_{\nu_{xL}}=f_{\nu_{yL}}=2/9,~f_{\nu_{eR}}=f_{\nu_{xR}}=f_{\nu_{yR}}=0)$ in Fig. 3, and any SFP and usual flavor conversions are

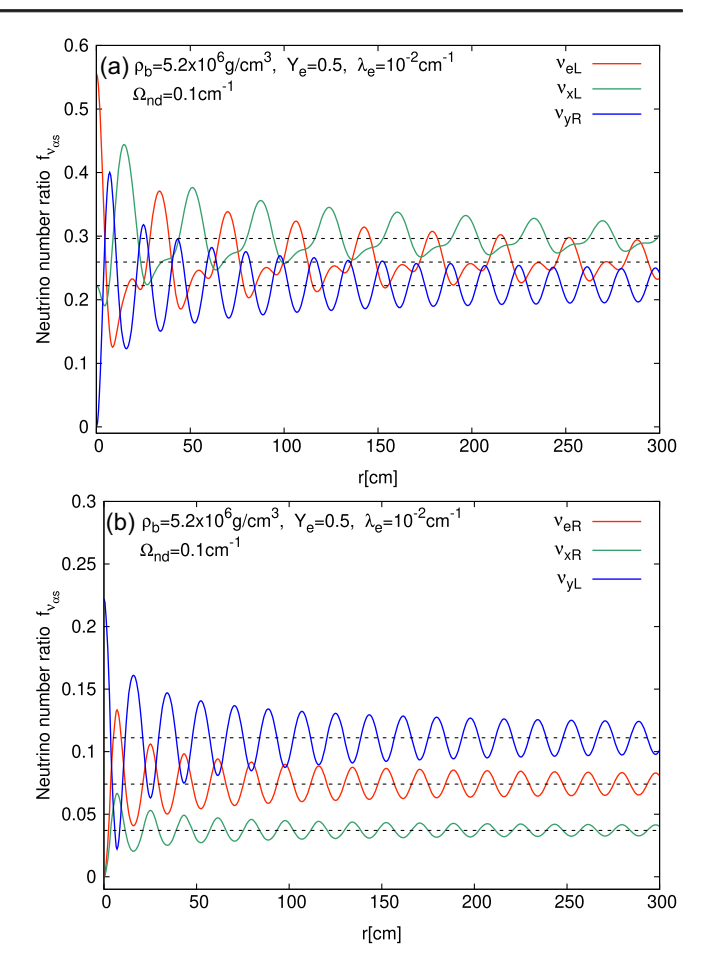


FIG. 2. (a) SFP of Dirac neutrinos with the nondiagonal term $\Omega_{\rm nd}=0.1~{\rm cm}^{-1}$ in Eq. (10) for $\lambda_e=0.1\Omega_{\rm nd}$ and $Y_e=0.5$ in the $\nu_{eL}-\nu_{xL}-\nu_{yR}$ sector. The dashed lines show equilibrium values $(n_{\nu_e}+n_{\nu_x})/3n_{\nu}=7/27$, $(2n_{\nu_e}+3n_{\nu_x})/6n_{\nu}=8/27$, and $(2n_{\nu_e}+n_{\nu_x})/6n_{\nu}=2/9$. (b) Result of the $\nu_{eR}-\nu_{xR}-\nu_{yL}$ sector. The dashed lines correspond to the values of $n_{\nu_y}/3n_{\nu}=2/27$, $n_{\nu_y}/6n_{\nu}=1/27$, and $n_{\nu_x}/2n_{\nu}=1/9$.

negligible. Such suppression due to the large matter potential is also confirmed in Majorana neutrinos [75]. In general, the magnetic field potential should be dominant among the potentials in the neutrino Hamiltonian for the significant SFP.

3. Case for $Y_e \sim 1/3$

The matter potentials λ_e and λ_n depend on both the baryon density and the electron fraction. Therefore, the matter suppression in Fig. 3 is sensitive to the value of the electron fraction, and the SFP is possible in some specific value of the electron fraction even in the large baryon density. Figure 4 shows the result in $\lambda_e = 10^2 \Omega_{\rm nd}$ with $\rho_{\rm b} = 7.8 \times 10^9 {\rm g/cm^3}$ and $Y_e = 1/3$. Evolutions of ν_{xL} , ν_{yL} , ν_{eR} , and ν_{xR} are negligible by the large matter potential λ_n . On the other hand, the SFP between ν_{eL} and ν_{vR} can avoid matter suppression. Such a SFP occurs

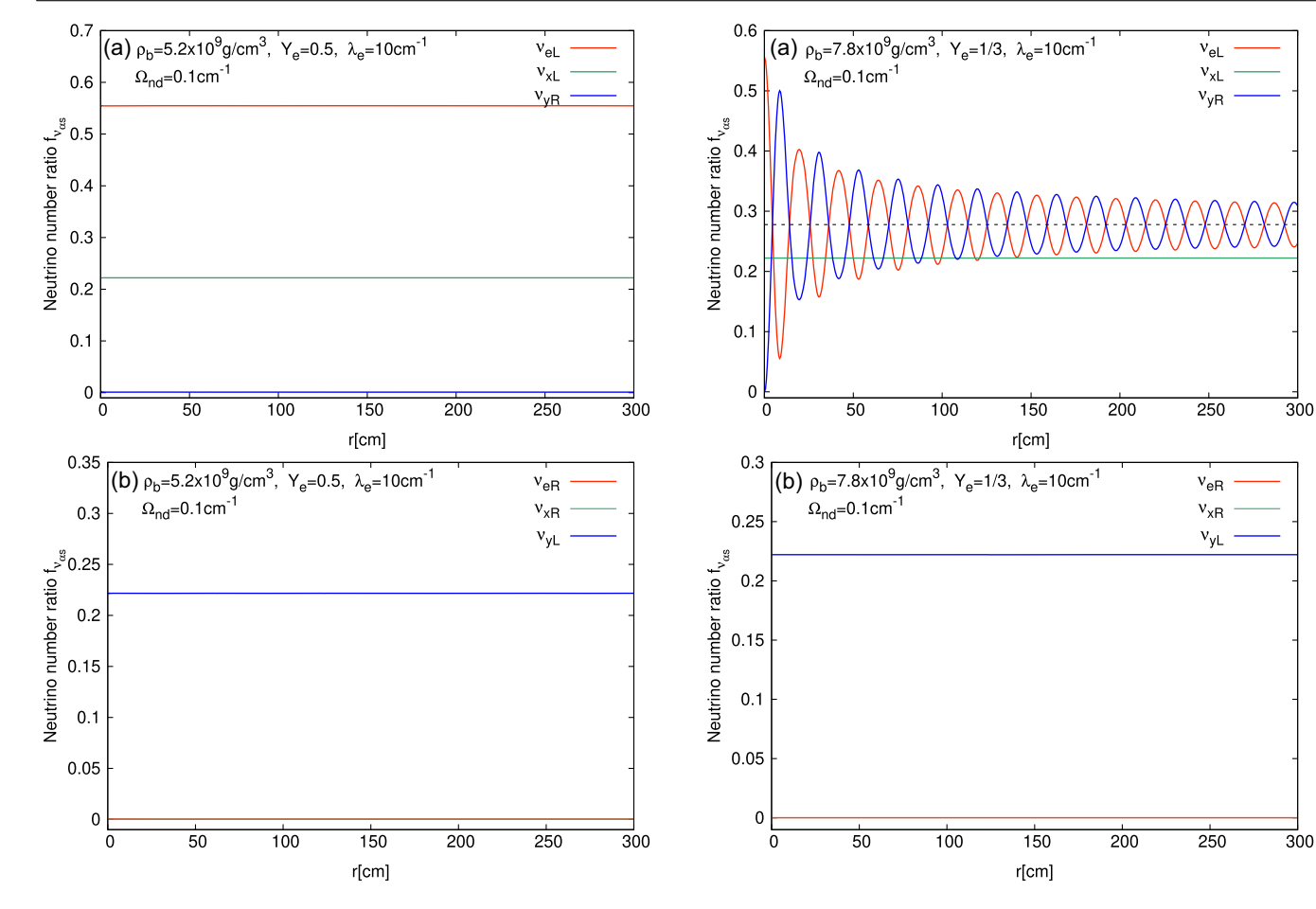


FIG. 3. SFP of Dirac neutrinos with the nondiagonal term $\Omega_{\rm nd}=0.1~{\rm cm^{-1}}~{\rm for}~\lambda_e=10^2\Omega_{\rm nd}$ and $Y_e=0.5$ both in the (a) ν_{eL} – ν_{xL} – ν_{yR} and (b) ν_{eR} – ν_{xR} – ν_{yL} sectors.

FIG. 4. SFP of Dirac neutrinos with the nondiagonal term $\Omega_{\rm nd}=0.1~{\rm cm^{-1}}$ for $\lambda_e=10^2\Omega_{\rm nd}$ and $Y_e=1/3$ both in the (a) $\nu_{eL}-\nu_{xL}-\nu_{yR}$ and (b) $\nu_{eR}-\nu_{xR}-\nu_{yL}$ sectors. The dashed line in (a) shows $n_{\nu_e}/2n_{\nu}=5/18$.

where $|\lambda_e - \lambda_n/2| \ll \Omega_{\rm nd}$ is satisfied. Note that $Y_e = 1/3$ satisfies this condition irrespective of the value of ρ_b . We remark that, for Majorana neutrinos, a similar SFP independent of the value of ρ_b occurs around $Y_e \sim 0.5$, where $|\lambda_e - \lambda_n| \ll \Omega_{\rm nd}$ is satisfied [75]. The mechanism of such ρ_b independent SFPs of Dirac neutrinos at $Y_e = 1/3$ is derived in Appendix A 3. More details on the differences between Dirac and Majorana neutrinos are discussed in Appendix B.

Almost the same discussion is possible for the right-handed antineutrinos by exchanging the sign of the matter potential $\lambda_{e(n)} \to -\lambda_{e(n)}$. Then, the equilibrium values of active neutrinos $[f_{\nu_a}^{\rm eq}, f_{\bar{\nu}_a}^{\rm eq} (\alpha = e, x, y)]$, such as in the dashed lines of Figs. 2 and 4, are connected with initial neutrino ratios $(f_{\nu_a}^i, f_{\bar{\nu}_a}^i)$ through a transition matrix $U_{\rm mag}^D$,

$$\begin{pmatrix} F_{\nu}^{\text{eq}} \\ F_{\bar{\nu}}^{\text{eq}} \end{pmatrix} = \begin{pmatrix} U_{\text{mag}}^{D} & 0 \\ 0 & U_{\text{mag}}^{D} \end{pmatrix} \begin{pmatrix} F_{\nu}^{i} \\ F_{\bar{\nu}}^{i} \end{pmatrix}, \tag{12}$$

$$F_{\nu}^{i(\text{eq})} = \begin{pmatrix} f_{\nu_e}^{i(\text{eq})} \\ f_{\nu_x}^{i(\text{eq})} \\ f_{\nu_x}^{i(\text{eq})} \end{pmatrix}, \tag{13}$$

$$F_{\bar{\nu}}^{i(\text{eq})} = \begin{pmatrix} f_{\bar{\nu}_e}^{i(\text{eq})} \\ f_{\bar{\nu}_x}^{i(\text{eq})} \\ f_{\bar{\nu}_y}^{i(\text{eq})} \end{pmatrix}, \tag{14}$$

where $U_{\rm mag}^D$ is a 3 × 3 transition matrix. The values of $U_{\rm mag}^D$ for three different extreme cases of neutrino potentials are shown in Table I. Figures 2–4 correspond to the cases of (1)–(3) in the table. Our demonstration assumes that both the matter and the magnetic field potentials are sufficiently large compared with the vacuum Hamiltonian. For the case of (2) in Table I, the SFP is suppressed, and the $U_{\rm mag}^D$ is equivalent to the 3 × 3 identity matrix. For the case of (1) and (3), the summation of $f_{\nu_a}^{\rm eq}(\alpha=e,x,y)$ is less than that

TABLE I. Transition matrix $U_{\rm mag}^D$ in Eq. (12) for Dirac neutrinos with the nondiagonal magnetic field potential $\Omega_{\rm nd}$ in Eq. (10) in three extreme cases of the matter and the magnetic field potentials. Case (3) is satisfied if $Y_e \sim 1/3$.

Case	$U_{ m mag}^D$
$(1) \lambda_e - \lambda_n/2 , \lambda_n \ll \Omega_{\rm nd}$	$\begin{pmatrix} \frac{1}{3} & \frac{1}{3} & 0\\ \frac{1}{3} & \frac{1}{2} & 0\\ 0 & 0 & \frac{1}{2} \end{pmatrix}$
(2) $ \lambda_e - \lambda_n/2 , \lambda_n \gg \Omega_{\rm nd}$	$\begin{pmatrix} 1 & 0 & 0 \\ 0 & 1 & 0 \\ 0 & 0 & 1 \end{pmatrix}$
(3) $ \lambda_e - \lambda_n/2 \ll \Omega_{\rm nd}, \lambda_n \gg \Omega_{\rm nd}$	$\begin{pmatrix} \frac{1}{2} & 0 & 0\\ 0 & 1 & 0\\ 0 & 0 & 1 \end{pmatrix}$

of $f_{\nu_a}^i$ due to the coupling with the right-handed neutrinos. Such a reduction of ratios of left-handed neutrinos is confirmed in antineutrinos, too.

As shown in Eq. (12), the neutrino and antineutrino sectors are decoupled from each other for Dirac neutrinos due to the decoupling as in Fig. 1(c). On the other hand, for Majorana neutrinos, the SFP occurs between neutrinos and antineutrinos as in Fig. 1(b). The equilibrium values of number ratios in three extreme cases are summarized in Eq. (B4) and Table II in Appendix B. Since the total number of active neutrinos ($\sum_{\alpha=e,x,y} f_{\nu_{\alpha}}^{\rm eq} + f_{\bar{\nu}_{\alpha}}^{\rm eq}$) is conserved through the SFP in Majorana neutrinos, the reduced neutrino flux could be a prominent feature that distinguishes both Dirac and Majorana neutrinos.

B. Diagonal magnetic field potential Ω_d

We discuss the SFP of Dirac neutrinos induced by the diagonal neutrino magnetic moment. We employ the same initial condition for the neutrino density matrix as Sec. III A and fix the strength of the magnetic field potential as $\Omega_d=0.1~\text{cm}^{-1}$ and $\Omega_{nd}=0~\text{cm}^{-1}$ in Eq. (10).

Figure 5 shows the result of the SFP induced by diagonal magnetic field potential $\Omega_{\rm d}$ with $\rho_{\rm b}=7.8\times 10^8~{\rm g/cm^3}$ and $Y_e=1/6$ resulting in $\lambda_e=5\Omega_{\rm d}$. The red lines are evolutions of $f_{\nu_{aL}}(\alpha=e,x,y)$, and the black lines are the summations of $f_{\nu_{aL}}+f_{\nu_{aR}}$ that are almost constant in the calculation. Such constant black lines suggest that the SFPs occur in the same flavors $\nu_{\alpha L}-\nu_{\alpha R}(\alpha=e,x,y)$ and are decoupled with each other. The dynamics of $\nu_{\alpha L}-\nu_{\alpha R}$ can be solved in the same way as the usual two flavor conversions. The result of Fig. 5(a) is consistent with the conversion $\nu_{eL}-\nu_{eR}$ in Ref. [4]. The equilibrium values of the left-handed neutrinos (dashed lines) are given by

$$f_{\nu_e}^{\text{eq}} = f_{\nu_e}^i \left\{ 1 - \frac{2\Omega_d^2}{(\lambda_e - \frac{\lambda_n}{2})^2 + 4\Omega_d^2} \right\}, \tag{15}$$

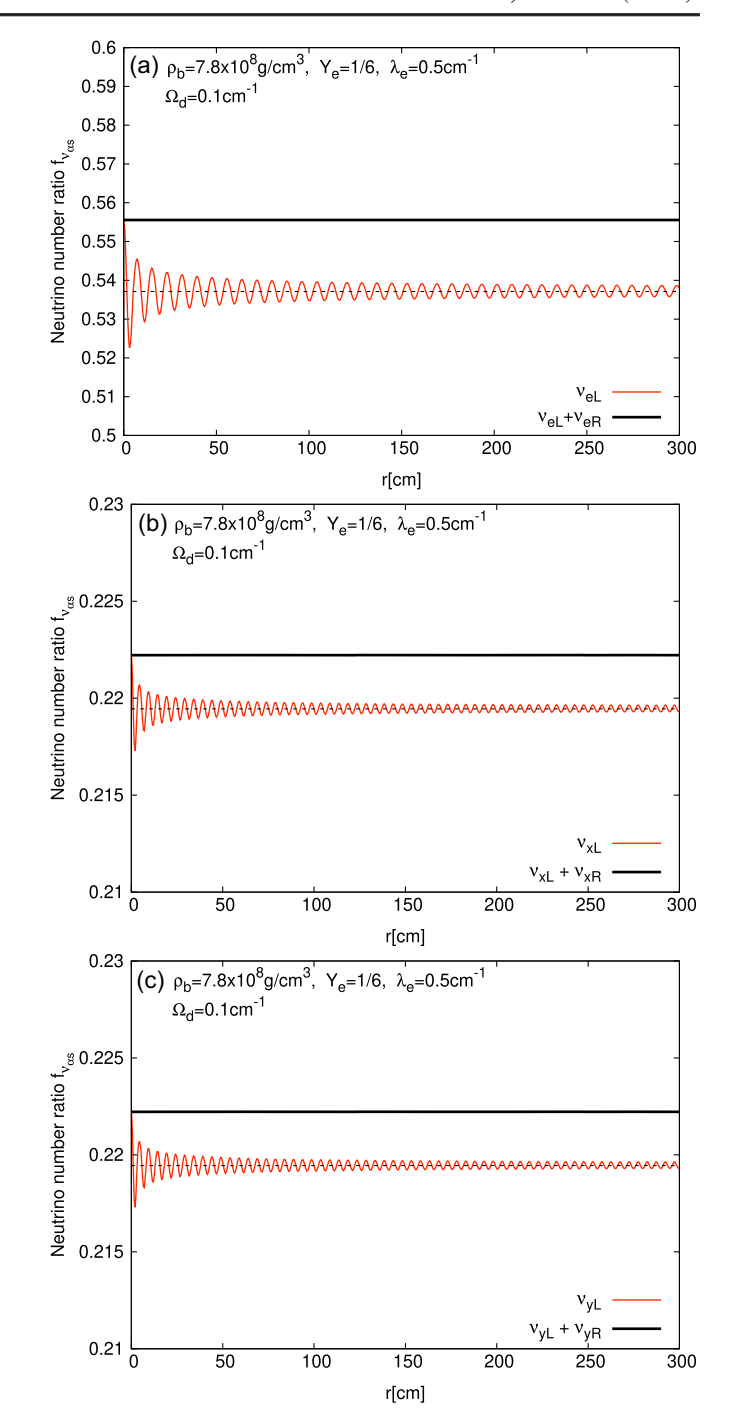


FIG. 5. SFP of Dirac neutrinos with the diagonal term $\Omega_{\rm d}=0.1~{\rm cm^{-1}}$ in Eq. (10) for $\lambda_e=5\Omega_{\rm d}$ and $Y_e=1/6$ in (a) $\nu_{eL}-\nu_{eR}$, (b) $\nu_{xL}-\nu_{xR}$, and (c) $\nu_{yL}-\nu_{yR}$ sector. The dashed lines correspond to Eqs. (15) and (16).

$$f_{\nu_{x(y)}}^{\text{eq}} = f_{\nu_{x(y)}}^{i} \left\{ 1 - \frac{2\Omega_{\text{d}}^{2}}{\left(\frac{\lambda_{n}}{2}\right)^{2} + 4\Omega_{\text{d}}^{2}} \right\}. \tag{16}$$

Similar relations are derived in the antineutrino sector. These equations show that conversions become maximum when the magnetic field potential is dominant,

 $|\lambda_e - \lambda_n/2|, \lambda_n \ll \Omega_{\rm d}$. Conversely, any SFP is negligible when the matter potentials are large, $|\lambda_e - \lambda_n/2|, \lambda_n \gg \Omega_{\rm d}$. The matter suppression does not occur in $\nu_{eL} - \nu_{eR}$ even in the large baryon density when the electron fraction is close to 1/3 because of $|\lambda_e - \lambda_n/2| \sim 0$. Our demonstration indicates that, in both the nondiagonal and diagonal cases, the strong magnetic field potentials larger than $|\lambda_e - \lambda_n/2|$ are necessary for the significant SFP of Dirac neutrinos.

C. Dirac vs Majorana in core-collapse supernovae

We investigate the possibility of the SFP of both Dirac and Majorana neutrinos in core-collapse supernovae with neutrino spectra and matter profiles obtained in a neutrino radiation-hydrodynamic simulation of the $11.2M_{\odot}$ progenitor model used in the demonstration for the Majorana neutrinos in ST21 [75].

As discussed in the previous sections, the strength of the magnetic field potential $\Omega_{\rm mag} = \mu_{\nu} B_T$ should be larger than $|\lambda_e - \lambda_n/2| (|\lambda_e - \lambda_n|)$ for the significant SFP of the Dirac (Majorana) neutrinos. To study the possibility of the SFP in core-collapse supernovae, we need to compare the magnetic field potential with other potentials in the neutrino Hamiltonian.

Near the PNS in core-collapse supernovae ($r \sim 10$ km), the neutrino-neutrino interaction could induce a non-negligible potential in the neutrino Hamiltonian. The strength of the neutrino-neutrino interactions at the radius from the center r could be estimated as (ST21 [75])

$$\zeta = \frac{\sqrt{2}G_F}{4\pi R_{\nu}^2} \left| \frac{L_{\nu_e}}{\langle E_{\nu_e} \rangle} - \frac{L_{\bar{\nu}_e}}{\langle E_{\bar{\nu}_e} \rangle} \right| \left(1 - \sqrt{1 - \left(\frac{R_{\nu}}{r}\right)^2} \right)^2, \quad (17)$$

where $\langle E_{\nu_i} \rangle$ and L_{ν_i} are the mean energy and luminosity of $\nu_i(\nu_i=\nu_e,\bar{\nu}_e)$ on the surface of the PNS $(r=R_{\nu})$. We define the value of R_{ν} at a radius where the baryon density corresponds to $\rho_{\rm b}=10^{11}~{\rm g/cm^3}$.

In the outer region of supernova matter $(r>10^3 \text{ km})$, the potentials of both matter and neutrino-neutrino interactions decrease, and the vacuum Hamiltonian $\Omega(E)$ in Eq. (4) becomes dominant. The strength of the vacuum Hamiltonian in our demonstration could be characterized by the atmospheric vacuum frequency $\omega=|\Delta m_{32}^2|/2E$, where E=10 MeV is a typical neutrino mean energy in core-collapse supernovae.

The magnetic field potential should be dominant among the potentials in the neutrino Hamiltonian for the significant SFP. Then, the necessary conditions for the SFPs of both Dirac and Majorana neutrinos are given by

$$\Omega_{\text{mag}} \ge \eta$$
(18)

$$\eta = \begin{cases}
\max\{\lambda_D, \zeta, \omega\} & \text{(Dirac)} \\
\max\{\lambda_M, \zeta, \omega\} & \text{(Majorana)},
\end{cases}$$
(19)

where $\lambda_D = |\lambda_e - \lambda_n/2|$ and $\lambda_M = |\lambda_e - \lambda_n|$. Here, η is the maximum value among the three strengths, and the difference between Dirac and Majorana neutrinos appears at λ_D and λ_M .

For the model of the magnetic field, we use a dipole magnetic field as employed in ST21 [75],

$$B_T = B_0 \left(\frac{R_\nu}{r}\right)^3,\tag{20}$$

where B_0 is the transverse magnetic field on the surface of PNS $(r = R_{\nu})$. The strength of the magnetic field potential $\Omega_{\rm mag} = \mu_{\nu} B_T$ is calculated with a fixed value of the neutrino magnetic moment, $\mu_{\nu} = 10^{-12} \mu_B$, satisfying the current experimental upper limit [7].

Figure 6 shows the strengths of the potentials and η in Eq. (19) for Dirac neutrinos at t = 125, 325, 525 ms after postbounce. The shaded region shows the interior of the PNS. The radius of the boundary corresponds to the PNS radius R_{ν} . The PNS radius becomes smaller as the explosion time passes due to the shrinking of the PNS. In all of the explosion time, the maximum strength η (blue line) is given by λ_D (red line) in $r > R_{\nu}$ except for a peak at $\lambda_D \sim 0$ where $Y_e = 1/3$ and $\eta = \zeta$ (green line) in Eq. (17). Near the surface of PNS, λ_D is large because of the dense and neutron-rich matter. On the other hand, the neutrino heating increases the value of the electron fraction outside the PNS, which results in the point of $\lambda_D \sim 0$ within r < 100 km. The baryon density decreases monotonously outside this point, and the sudden decrease of λ_D around 200 km in Fig. 6(a) corresponds to the propagating shock front.

The values of $\Omega_{\rm mag}$ in Fig. 6 (magenta lines) are obtained with the typical magnetic field of magnetars $B_0=10^{14}~{\rm G}$ in Eq. (20). The magenta lines can move upwards with large B_0 , keeping the same slope due to the same radial dependence of Eq. (20). The necessary condition in Eq. (18) is satisfied where the magenta lines are larger than the blue lines. The magenta lines in Fig. 6 are always smaller than the blue lines, which indicates that $B_0=10^{14}~{\rm G}$ is insufficient to satisfy Eq. (18). For a more quantitative discussion, we introduce a minimum magnetic field on the surface of PNS,

$$B_{0,\min}(r) = \frac{r^3}{\mu_\nu R_\nu^3} \eta. \tag{21}$$

Equation (18) is satisfied at the radius r when $B_0 > B_{0,\min}(r)$. Figure 7 shows the results of Eq. (21) at different explosion times of Fig. 6. The $B_{0,\min}(r)$ becomes minimum at the point $\lambda_D \sim 0$ at any explosion time. The minimum values are 2.24×10^{14} , 1.86×10^{14} , 2.23×10^{14} G at t = 125, 325, 525 ms after postbounce. The strong magnetic field $B_0 > 10^{16}$ G is required for Eq. (18) in regions other than such resonance points.

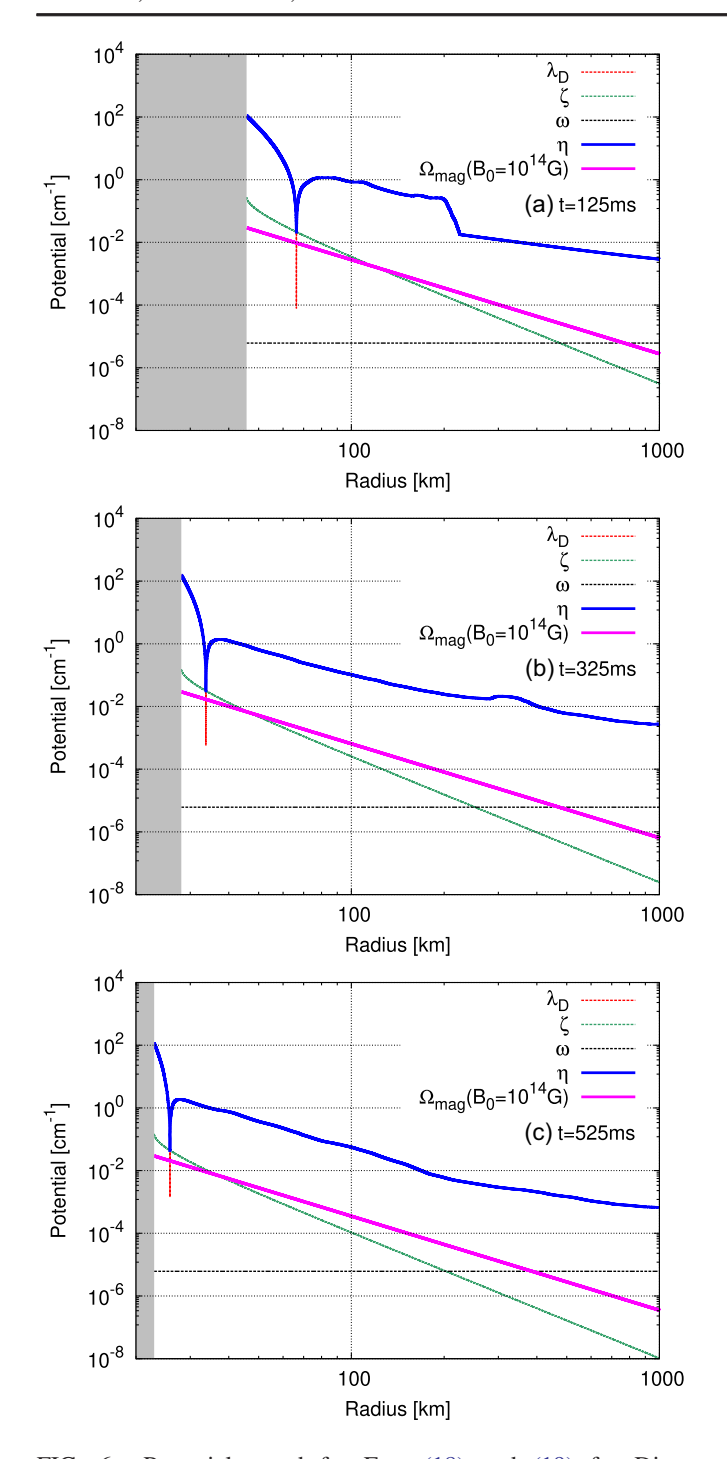


FIG. 6. Potentials used for Eqs. (18) and (19) for Dirac neutrinos at different explosion times after postbounce (t = 125, 325, 525 ms). The shaded region shows the interior of the PNS.

Figure 8 shows profiles of the potentials for Majorana neutrinos with different time snapshots, as in Fig. 6. In Fig. 8(a), at t=125 ms, the maximum strength η (blue line) is equal to λ_M (red line) near the PNS radius, and the λ_M decreases significantly outside the shock front (r>200 km) due to the small baryon density and $Y_e\sim0.5$ in the Si layer. Then, the η is determined by ζ (green

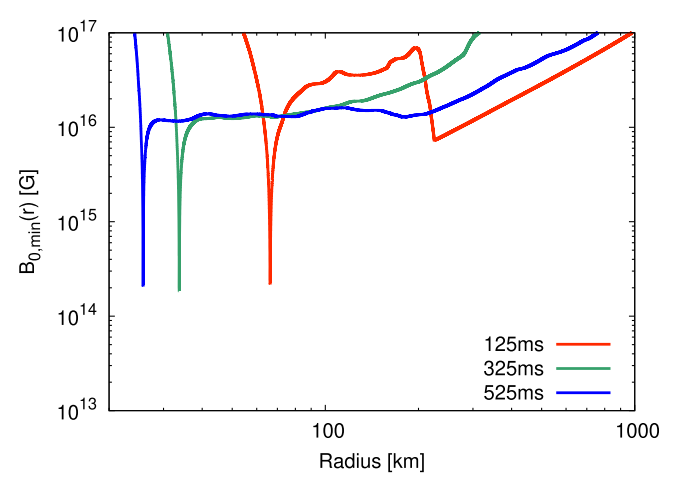


FIG. 7. Radial profile of Eq. (21) for Dirac neutrinos.

line) and ω (black line) in such outer regions. The SFP around 800 km would depend on the neutrino mass hierarchy because ω becomes maximum and comparable with Ω_{mag} . Such hierarchy dependence does not appear in Dirac neutrinos within 1000 km because $\omega < \eta$ at any radius, as shown in Fig. 6(a). This does not happen even when r > 1000 km because $\omega \gg \Omega_{\rm mag}$. In Fig. 8(b), at t = 325 ms, there are several peaks of $\lambda_M \sim 0$ (red line) where $Y_e = 0.5$. Such peaks are favorable to satisfy Eq. (18). The small λ_M enables the crossing of $\Omega_{\rm mag}$ (magenta lines) and η (blue lines) in Figs. 8(a) and 8(b). Therefore, $B_0 = 10^{14}$ G is sufficient to satisfy Eq. (18) for Majorana neutrinos. On the other hand, there are no peaks of $\lambda_M \sim 0$ at t = 525 ms as in Fig. 8(c) because the electron fraction is not close to 0.5. Then, there is no crossing of $\Omega_{\rm mag}$ (magenta line) and η (blue line) in this explosion phase.

The result of Eq. (21) for Majorana neutrinos is shown in Fig. 9. As shown in the case of 125 ms (red line), the minimum value is given by 2.34×10^{13} G at r=474 km in the Si layer outside the shock wave. After the shock propagation, $B_{0,\min}(r)$ in the shock-heated material becomes small at the point $Y_e=0.5$, and the minimum value at 325 ms (green line) is given by 1.72×10^{13} G at r=222 km. There is no point $Y_e=0.5$ at 525 ms, and $B_{0,\min}(r)$ is larger than 10^{14} G.

The minimum value of Eq. (21) outside the PNS radius,

$$B_{\rm cr} = \min_{r \ge R_{\nu}} \{ B_{0,\min}(r) \}, \tag{22}$$

could be regarded as a critical magnetic field on the surface of PNS for the SFP at the explosion time.

Figure 10 shows the result of Eq. (22) at the different explosion times for both Dirac and Majorana neutrinos. The value for Dirac neutrinos is larger than 10^{14} G. As shown in Fig. 7, the $B_{0,\min}(r)$ for Dirac neutrinos becomes minimum at the radius of $Y_e \sim 1/3$. Such a specific radius

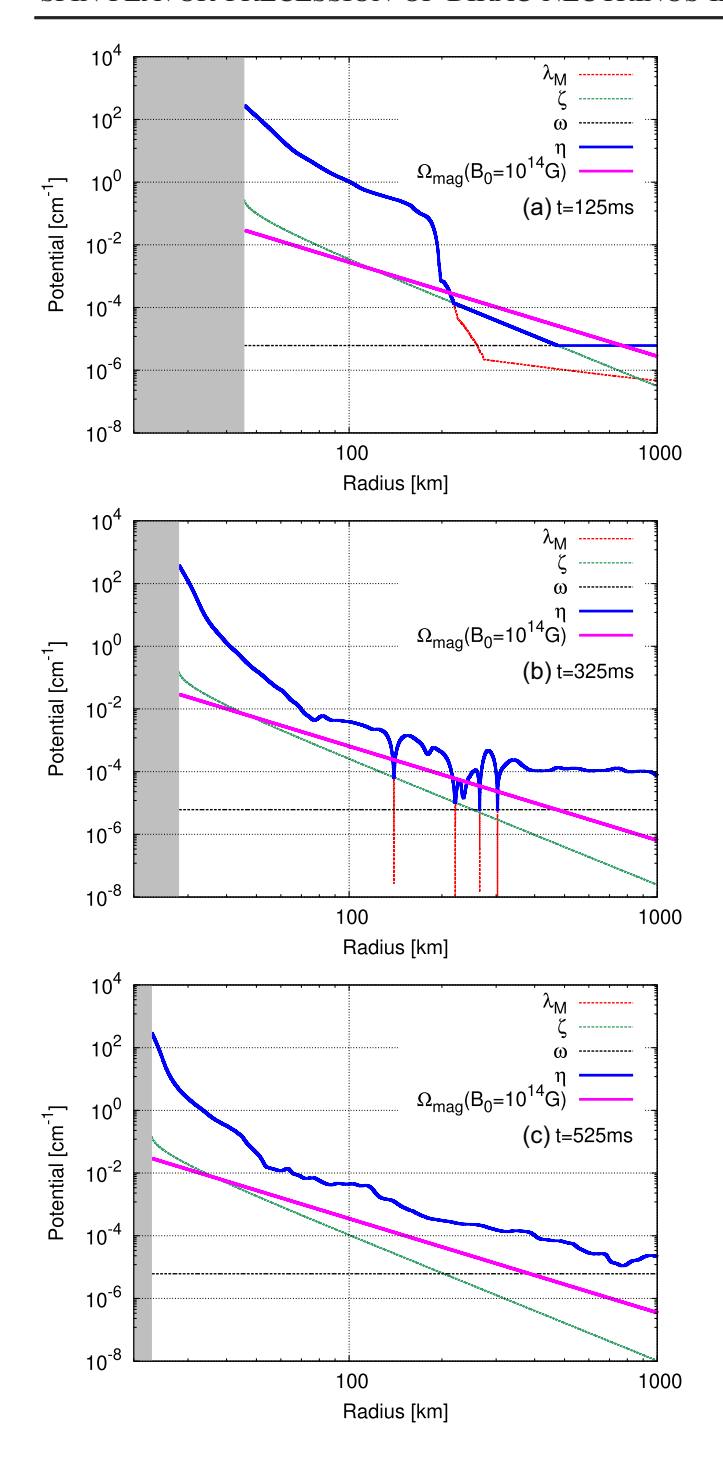


FIG. 8. Potentials for the Majorana neutrinos in Eqs. (18) and (19) at t = 125, 325, 525 ms after postbounce, as in Fig. 6.

appears near the PNS radius inside the shock-heated material. We remark that the supernova matter profiles used in Figs. 6 and 8 are obtained by averaging the contribution from the various directions with the polar angle $\Theta \in [0, \pi]$ of the 2D hydrodynamic simulation. Hence, the angular dependence on the profile of Y_e is also averaged out in our analysis. In addition, our demonstration implicitly assumes the strength of the dipole magnetic field

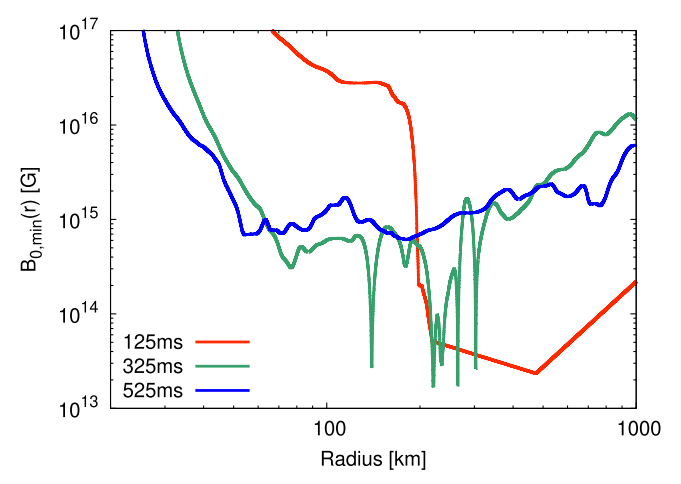


FIG. 9. Radial profile of Eq. (21) for Majorana neutrinos.

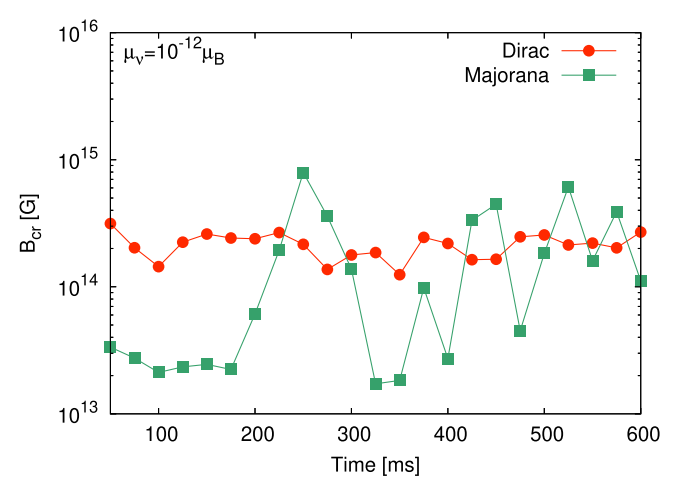


FIG. 10. Critical magnetic field on the surface of the PNS in Eq. (22) for both Dirac and Majorana neutrinos.

of the equator of the PNS ($\Theta=\pi/2$) and ignores the dependence of $\sin\Theta$ on Eq. (20) [64]. Such a Θ dependence implies that the spin precession is less likely to occur in the polar direction ($\Theta\sim0$) due to the larger critical magnetic field.

As shown in Fig. 10, the value of $B_{\rm cr}$ for Majorana neutrinos is less than 10^{14} G and smaller than those of Dirac neutrinos in t < 200 ms. In this early explosion phase, as in Fig. 8(a), the value of λ_M decreases significantly outside the shock front where ρ_b is small and Y_e is close to 0.5 due to many α elements, which results in the small $B_{\rm cr}$. The SFP of Majorana neutrinos is more favorable than those of Dirac neutrinos in the early phase before the shock wave has reached the α element layer.

While propagating outwards, the shock wave heats the material of outer layers and changes the value of Y_e . In the later explosion phase ($t \ge 200$ ms), $B_{\rm cr}$ for Majorana neutrinos fluctuates in the range 10^{13} – 10^{15} G, although the value for Dirac neutrinos is roughly constant. Such fluctuations originated from several peaks of $\lambda_M \sim 0$ as in

Fig. 8(b) and the absence of peaks as in Fig. 8(c). The value of Y_e is particularly uncertain around 0.5 and dependent on the neutrino radiation transport scheme used in the supernova hydrodynamic simulation. More elaborate neutrino transport would enable a more detailed analysis of Majorana neutrinos in the later explosion phase.

In this study, we primarily focused on delineating the criteria for SFP and omitted an elaboration of the anticipated neutrino event rate and spectrum. To predict them, we need to investigate other aspects of neutrino oscillations, especially collective neutrino oscillations. In particular, the implications of fast flavor conversions in supernova environments are actively debated (e.g., [77–80]). We remark that, instead of the simple neutrino emission model used in our demonstration, neutrino angular distributions dependent on neutrino species are required for the calculation of the SFP that considers the fast flavor conversions. A comprehensive study encompassing both SFP and fast flavor conversions is deferred to future work.

IV. CONCLUSION

We calculate the SFP of Dirac neutrinos induced by the coupling of neutrino magnetic moments and magnetic fields in dense matter. This work is an extension of our previous work for neutrino-antineutrino oscillations of Majorana neutrinos [75]. We demonstrate the SFP of Dirac neutrinos for both diagonal and nondiagonal neutrino magnetic moments. The SFP occurs significantly when the matter potentials are negligible compared with the magnetic field potential. The large baryon density tends to prevent the SFP. However, the SFP is possible in ν_e even with the large baryon density when the electron fraction is close to 1/3.

Finally, we verify the possibility of the SFP of both Dirac and Majorana neutrinos in core-collapse supernovae based on the necessary condition of the SFP derived from our demonstrations by using simulation data of the $11.2M_{\odot}$ progenitor model with a fixed value of the neutrino magnetic moment $\mu_{\nu}=10^{-12}\mu_{B}$. In the case of Dirac neutrinos, the required magnetic field on the surface of the PNS for the SFP is a few 10^{14} G at any explosion time. The required magnetic field for Majorana neutrinos is a few 10^{13} G in the early explosion phase before the shock reaches the Si layer. On the other hand, in the later explosion phase, the magnetic field fluctuates in the range 10^{13} – 10^{15} G, which is sensitive to the scheme of the neutrino transport used in hydrodynamic simulations.

ACKNOWLEDGMENTS

We thank H. Nagakura for stimulating discussions. This work was carried out under the auspices of the National Nuclear Security Administration of the U.S. Department of Energy at Los Alamos National Laboratory under Contract No. 89233218CNA000001. This study was supported in

part by JSPS/MEXT KAKENHI Grants No. JP17H06364, No. JP21H01088, No. JP22H01223, No. JP23H01199, and No. JP23K03400. This work was also supported by the NINS program for the cross-disciplinary study (Grants No. 01321802 and No. 01311904) on Turbulence, Transport, and Heating Dynamics in Laboratory and Solar/Astrophysical Plasmas: "SoLaBo-X." This work was also supported in part by U.S. National Science Foundation Grants No. PHY-2020275 and No. PHY-2108339. Numerical computations were carried out on the PC cluster and Cray XC50 at the Center for Computational Astrophysics, National Astronomical Observatory of Japan. This research was also supported by MEXT as "Program for Promoting researches on the Supercomputer Fugaku" (Structure and Evolution of the Universe Unraveled by Fusion of Simulation and AI; Grant No. JPMXP1020230406) and JICFuS.

APPENDIX A: MATTER SUPPRESSION WITH Ω_{nd}

Following a similar approach as in ST21 [75], we derive the equilibrium values (dashed lines) in Figs. 2 and 4. We solve Eq. (1) with $\theta=0$ assuming the dense matter $H_L \sim V_{\rm mat},\ H_R \sim 0$, and the negligible diagonal neutrino magnetic moment $\Omega_{\rm d}=0$ in Eq. (10). The term θ in Eq. (2) is dropped hereafter. Then, the equation of motion in Eq. (1) is decomposed by

$$\partial_r \rho_L \sim -i [V_{\rm mat}, \rho_L] - i (V_{\rm mag} X^\dagger - X V_{\rm mag}^\dagger), \quad ({\rm A1})$$

$$\partial_r \rho_R \sim -i (V_{\rm mag}^\dagger X - X^\dagger V_{\rm mag}), \tag{A2} \label{eq:A2}$$

$$\partial_r X \sim -i(V_{\rm mat}X + V_{\rm mag}\rho_R - \rho_L V_{\rm mag}), \eqno(A3)$$

where $\partial_r = \partial/\partial_r$. The above equations of motion in the $e - \mu - \tau$ basis can be described in the e - x - y basis through the transformation of matrices such as

$$\begin{aligned} V_{\text{mat}}' &= R^T(\theta_{23}) V_{\text{mat}} R(\theta_{23}) \\ &= V_{\text{mat}}, \end{aligned} \tag{A4}$$

$$V'_{\text{mag}} = R^{T}(\theta_{23})V_{\text{mag}}R(\theta_{23})$$

$$= \Omega_{\text{nd}} \begin{pmatrix} 0 & 0 & \sqrt{2} \\ 0 & 0 & 1 \\ -\sqrt{2} & -1 & 0 \end{pmatrix}, \quad (A5)$$

$$R(\theta_{23}) = \begin{pmatrix} 1 & 0 & 0 \\ 0 & \cos \theta_{23} & \sin \theta_{23} \\ 0 & -\sin \theta_{23} & \cos \theta_{23} \end{pmatrix}, \quad (A6)$$

where $\theta_{23} = \pi/4$. Here, we comment that the matrix components of Eq. (A4) in ST21 [75] should be corrected

as Eq. (A5) for a more precise discussion on Majorana neutrinos, although the same equilibrium values of neutrino-antineutrino oscillations are derived with Eq. (A5). Following the matrix transformation of Eqs. (A4)–(A6), the evolutions of the matrix components of the neutrino density matrices in the e-x-y basis are given by

$$\partial_r \rho_{\text{Lee}} = -2\sqrt{2}\Omega_{\text{nd}} X_{ev,i},$$
 (A7)

$$\partial_r \rho_{Lxx} = -2\Omega_{\rm nd} X_{xv,i},\tag{A8}$$

$$\partial_r \rho_{Ryy} = 2\sqrt{2}\Omega_{nd} X_{ey,i} + 2\Omega_{nd} X_{xy,i}, \tag{A9}$$

$$\begin{split} \partial_r \rho_{Lex} &= -i \lambda_e \rho_{Lex} \\ &- i \Omega_{\rm nd} (-X_{ey} + \sqrt{2} X_{xy}^*), \end{split} \tag{A10}$$

$$\partial_r \rho_{Ree} = -2\sqrt{2}\Omega_{\rm nd} X_{ye,i},\tag{A11}$$

$$\partial_r \rho_{Rxx} = -2\Omega_{\rm nd} X_{vx,i},\tag{A12}$$

$$\partial_r \rho_{Lvv} = 2\sqrt{2}\Omega_{nd} X_{ve,i} + 2\Omega_{nd} X_{vx,i}, \qquad (A13)$$

$$\partial_r \rho_{Rex} = -i\Omega_{\rm nd}(X_{ve}^* - \sqrt{2}X_{vx}^*),\tag{A14}$$

where $X_{\alpha\beta,i} = \text{Im}X_{\alpha\beta}(\alpha, \beta = e, x, y)$. From these equation of motions, conservation laws are obtained,

$$\rho_{Lee} + \rho_{Lxx} + \rho_{Ryy} = \text{const}, \tag{A15}$$

$$\rho_{Ree} + \rho_{Rxx} + \rho_{Lyy} = \text{const}, \tag{A16}$$

which represent a decoupling of the $\nu_{eL} - \nu_{xL} - \nu_{yR}$ and $\nu_{eR} - \nu_{xR} - \nu_{yL}$ sectors. We confirm that these conservation laws are numerically satisfied in Figs. 2–4. From Eq. (A3), the evolution of X is obtained, and the evolutions of X_{ey} , X_{xy} , X_{ye} , X_{yx} are given by

$$\partial_r X_{ey} = -i \left(\lambda_e - \frac{\lambda_n}{2} \right) X_{ey}$$

$$- i \Omega_{\text{nd}} \{ \sqrt{2} (\rho_{Ryy} - \rho_{Lee}) - \rho_{Lex} \}, \qquad (A17)$$

$$\partial_r X_{xy} = -i\left(-\frac{\lambda_n}{2}\right) X_{xy} - i\Omega_{\rm nd}(\rho_{Ryy} - \rho_{Lxx} - \sqrt{2}\rho_{Lex}^*), \tag{A18}$$

$$\partial_r X_{ye} = -i\left(-\frac{\lambda_n}{2}\right) X_{ye} -i\Omega_{nd} \{\sqrt{2}(\rho_{Lyy} - \rho_{Ree}) - \rho_{Rex}^*\}, \qquad (A19)$$

$$\partial_r X_{yx} = -i\left(-\frac{\lambda_n}{2}\right) X_{yx} -i\Omega_{\rm nd}(\rho_{Lyy} - \rho_{Rxx} - \sqrt{2}\rho_{Rex}).$$
 (A20)

The above equations are needed to close Eqs. (A7)–(A14), and they are solved analytically in the extreme cases as in Table I.

1. Case of $|\lambda_e - \lambda_n/2|$, $\lambda_n \ll \Omega_{\rm nd}$

In this case, the discussions on both the $\nu_{eL} - \nu_{xL} - \nu_{yR}$ and $\nu_{eR} - \nu_{xR} - \nu_{yL}$ sectors are almost the same. Then, we only focus on the derivation in the $\nu_{eL} - \nu_{xL} - \nu_{yR}$ sector by using Eqs. (A7)–(A10), (A17), and (A18). The second derivatives of $X_{ey,i}$ and $X_{xy,i}$ are described by

$$\partial_r^2 \begin{pmatrix} \sqrt{2} X_{ey,i} \\ X_{xy,i} \end{pmatrix} \sim -3\Omega_{\text{nd}}^2 \begin{pmatrix} 3 & 2 \\ 1 & 2 \end{pmatrix} \begin{pmatrix} \sqrt{2} X_{ey,i} \\ X_{xy,i} \end{pmatrix}.$$
 (A21)

The above equation can be solved with the initial diagonal densities $\rho_{sa\alpha}=\rho_{sa\alpha}^0(\alpha=e,x,y,s=L,R)$ and the negligible correlation X=0 at r=0 as done in ST21 [75]. The diagonal components $\rho_{sa\alpha}$ are composed of two modes, $\cos(\sqrt{3}\Omega_{\rm nd}r)$ and $\cos(2\sqrt{3}\Omega_{\rm nd}r)$, oscillating around the equilibrium values below,

$$\rho_{Lee}^{\text{eq}} = \frac{\rho_{Lee}^0 + \rho_{Lxx}^0 + \rho_{Ryy}^0}{3}, \tag{A22}$$

$$\rho_{Lxx}^{\text{eq}} = \frac{2\rho_{Lee}^0 + 3\rho_{Lxx}^0 + \rho_{Ryy}^0}{6},$$
 (A23)

$$\rho_{Ryy}^{\text{eq}} = \frac{2\rho_{Lee}^0 + \rho_{Lxx}^0 + 3\rho_{Ryy}^0}{6}.$$
 (A24)

The dashed lines in Fig. 2(a) are reproduced with the above equations by imposing $\rho_{Lee}^0 = n_{\nu_e}/n_{\nu}$, $\rho_{Lxx}^0 = n_{\nu_x}/n_{\nu}$, and $\rho_{Ryy}^0 = 0$. The equilibrium values of the $\nu_{eR} - \nu_{xR} - \nu_{yL}$ sector in Fig. 2(b) are given by the replacements of $\rho_L \to \rho_R$ and $\rho_R \to \rho_L$ in Eqs. (A22)–(A24).

2. Case of $|\lambda_e - \lambda_n/2|$, $\lambda_n \gg \Omega_{\rm nd}$

The second derivatives of X_{ey} and X_{xy} are written as

$$\partial_r^2 X_{ey} \sim -\left(\lambda_e - \frac{\lambda_n}{2}\right)^2 X_{ey},$$
 (A25)

$$\partial_r^2 X_{xy} \sim -\frac{\lambda_n^2}{4} X_{xy}. \tag{A26}$$

These equations are solved analytically. However, the negligible correlation X = 0 at r = 0 and Eqs. (A17) and (A18) indicate $X_{ey} = X_{xy} = 0$ irrespective of the radius, which results in no SFP as in Fig. 3. We can show

negligible SFP in the $\nu_{eR} - \nu_{xR} - \nu_{yL}$ sector in the same way.

3. Case of
$$|\lambda_e - \lambda_n/2| \ll \Omega_{\rm nd}$$
, $\lambda_n \gg \Omega_{\rm nd}$

In this case, there is no SFP in the $\nu_{eR} - \nu_{xR} - \nu_{yL}$ sector as in Appendix A 2. Such negligible SFP is consistent with the numerical result in Fig. 4(b). In addition, X_{xy} and ρ_{Lex} are negligible due to large λ_n and λ_e . From Eq. (A8), the value of ρ_{Lxx} is constant and decoupled from the spin precession. Such a decoupling of ν_{xL} is confirmed numerically in Fig. 4(a). The second derivative of X_{ey} is given by

$$\partial_r^2 X_{ey} \sim -8\Omega_{\rm nd}^2 X_{ey}.$$
 (A27)

Following the same procedure as in Appendix A 1, ρ_{Lee} and ρ_{Ryy} are described by a single mode of $\cos(2\sqrt{2}\Omega_{\rm nd}r)$, and the equilibrium value is written as

$$\rho_{Lee}^{\text{eq}} = \rho_{Ryy}^{\text{eq}} = \frac{\rho_{Lee}^0 + \rho_{Ryy}^0}{2},$$
(A28)

which reproduces the dashed line in Fig. 4(a) with $\rho_{Lee}^0 = n_{\nu_e}/n_{\nu}$ and $\rho_{Ryy}^0 = 0$.

APPENDIX B: EQUILIBRIUM VALUES FOR MAJORANA NEUTRINOS

A similar discussion can be made as in Appendix A for Majorana neutrinos by replacing $H_R \to -V_{\rm mat}$ and $\rho_R \to \bar{\rho}_R$ and solving the equations of motion below,

$$\partial_r \rho_L \sim -i[V_{\text{mat}}, \rho_L] - i(V_{\text{mag}} X^{\dagger} - X V_{\text{mag}}^{\dagger}), \quad (B1)$$

$$\partial_r \bar{\rho}_R \sim i [V_{\rm mat}, \bar{\rho}_R] - i (V_{\rm mag}^\dagger X - X^\dagger V_{\rm mag}), \qquad ({\rm B2})$$

$$\partial_r X \sim -i(V_{\text{mat}}X + XV_{\text{mat}} + V_{\text{mag}}\bar{\rho}_R - \rho_L V_{\text{mag}}),$$
 (B3)

where X is a correlation matrix between neutrinos and antineutrinos. The connection between equilibrium and initial fluxes in Eqs. (13) and (14) is given by

TABLE II. Transition matrix U_{mag}^{M} in Eq. (B4) for Majorana neutrinos in three extreme cases. Case (3) is satisfied if $Y_{e} \sim 0.5$.

Case	$U_{ m mag}^M$
(1) $ \lambda_e - \lambda_n , \lambda_n \ll \Omega_{\rm nd}$	$\begin{pmatrix} \frac{1}{3} & \frac{1}{3} & 0 & 0 & 0 & \frac{1}{3} \\ \frac{1}{3} & \frac{1}{2} & 0 & 0 & 0 & \frac{1}{6} \\ 0 & 0 & \frac{1}{2} & \frac{1}{3} & \frac{1}{6} & 0 \\ 0 & 0 & \frac{1}{3} & \frac{1}{3} & \frac{1}{3} & 0 \\ 0 & 0 & \frac{1}{6} & \frac{1}{3} & \frac{1}{2} & 0 \\ \frac{1}{3} & \frac{1}{6} & 0 & 0 & 0 & \frac{1}{2} \end{pmatrix}$
(2) $ \lambda_e - \lambda_n , \lambda_n \gg \Omega_{\rm nd}$	$\begin{pmatrix} 1 & 0 & 0 & 0 & 0 & 0 \\ 0 & 1 & 0 & 0 & 0 & 0 \\ 0 & 0 & 1 & 0 & 0 & 0 \\ 0 & 0 & 0 & 1 & 0 & 0 \\ 0 & 0 & 0 & 0 & 1 & 0 \\ 0 & 0 & 0 & 0 & 0 & 1 \end{pmatrix}$
(3) $ \lambda_e - \lambda_n \ll \Omega_{\rm nd}, \lambda_n \gg \Omega_{\rm nd}$	$\begin{pmatrix} \frac{1}{2} & 0 & 0 & 0 & 0 & \frac{1}{2} \\ 0 & 1 & 0 & 0 & 0 & 0 \\ 0 & 0 & \frac{1}{2} & \frac{1}{2} & 0 & 0 \\ 0 & 0 & \frac{1}{2} & \frac{1}{2} & 0 & 0 \\ 0 & 0 & 0 & 0 & 1 & 0 \\ \frac{1}{2} & 0 & 0 & 0 & 0 & \frac{1}{2} \end{pmatrix}$

$$\begin{pmatrix} F_{\nu}^{\text{eq}} \\ F_{\bar{\nu}}^{\text{eq}} \end{pmatrix} = U_{\text{mag}}^{M} \begin{pmatrix} F_{\nu}^{i} \\ F_{\bar{\nu}}^{i} \end{pmatrix}, \tag{B4}$$

where $U_{\rm mag}^M$ is a 6×6 transition matrix due to the mixing of three flavors of neutrinos and those of antineutrinos as in Fig. 1(b). The values of three extreme cases for Majorana neutrinos are summarized in Table II. Numerical results for Majorana neutrinos are shown in ST21 [75], and the equilibrium values of the three extreme cases are reproduced by $f_{\nu_x}^i = f_{\nu_x}^i = f_{\bar{\nu}_x}^i = f_{\bar{\nu}_y}^i$ in Eq. (B4). We remark that $V_{\rm mat}X + XV_{\rm mat}$ in Eq. (B3) induces a frequency $\lambda_e - \lambda_n$ in Table II. On the other hand, for Dirac neutrinos, a frequency $\lambda_e - \lambda_n/2$ in Table I comes from $V_{\rm mat}X$ in Eq. (A3). This difference for Majorana and Dirac neutrinos is the origin of the different necessary conditions in Eq. (19).

^[1] A. B. Balantekin and B. Kayser, On the properties of neutrinos, Annu. Rev. Nucl. Part. Sci. 68, 313 (2018).

^[2] M. J. Dolinski, A. W. P. Poon, and W. Rodejohann, Neutrinoless double-beta decay: Status and prospects, Annu. Rev. Nucl. Part. Sci. 69, 219 (2019).

^[3] C. Giunti and C. W. Kim, Fundamentals of Neutrino Physics and Astrophysics (Oxford University Press, 2007), https://doi.org/10.1093/acprof:oso/9780198508717.001.0001.

^[4] C.-S. Lim and W. J. Marciano, Resonant spin-flavor precession of solar and supernova neutrinos, Phys. Rev. D 37, 1368 (1988).

- [5] E. K. Akhmedov, Resonant amplification of neutrino spin rotation in matter and the solar neutrino problem, Phys. Lett. B 213, 64 (1988).
- [6] A. B. Balantekin, P. J. Hatchell, and F. Loreti, Matter enhanced spin flavor precession of solar neutrinos with transition magnetic moments, Phys. Rev. D 41, 3583 (1990).
- [7] E. Aprile *et al.* (XENON Collaboration), Search for new physics in electronic recoil data from XENONnT, Phys. Rev. Lett. **129**, 161805 (2022).
- [8] H. Bonet *et al.* (CONUS Collaboration), First upper limits on neutrino electromagnetic properties from the CONUS experiment, Eur. Phys. J. C **82**, 813 (2022).
- [9] P. Coloma, I. Esteban, M. C. Gonzalez-Garcia, L. Larizgoitia, F. Monrabal, and S. Palomares-Ruiz, Bounds on new physics with data of the Dresden-II reactor experiment and COHERENT, J. High Energy Phys. 05 (2022) 037.
- [10] K. Abe *et al.* (XMASS Collaboration), Search for exotic neutrino-electron interactions using solar neutrinos in XMASS-I, Phys. Lett. B **809**, 135741 (2020).
- [11] S. Arceo-Díaz, K. P. Schröder, K. Zuber, and D. Jack, Constraint on the magnetic dipole moment of neutrinos by the tip-RGB luminosity in ω-Centauri, Astropart. Phys. 70, 1 (2015).
- [12] F. Capozzi and G. Raffelt, Axion and neutrino bounds improved with new calibrations of the tip of the red-giant branch using geometric distance determinations, Phys. Rev. D 102, 083007 (2020).
- [13] K. Mori, A. B. Balantekin, T. Kajino, and M. A. Famiano, Elimination of the blue loops in the evolution of intermediate-mass stars by the neutrino magnetic moment and large extra dimensions, Astrophys. J. 901, 115 (2020).
- [14] N. Vassh, E. Grohs, A. B. Balantekin, and G. M. Fuller, Majorana neutrino magnetic moment and neutrino decoupling in big bang nucleosynthesis, Phys. Rev. D 92, 125020 (2015).
- [15] E. Grohs and A. B. Balantekin, Implications on cosmology from Dirac neutrino magnetic moments, Phys. Rev. D 107, 123502 (2023).
- [16] A. Burrows, L. Dessart, E. Livne, C. D. Ott, and J. Murphy, Simulations of magnetically driven supernova and hypernova explosions in the context of rapid rotation, Astrophys. J. 664, 416 (2007).
- [17] T. Takiwaki, K. Kotake, and K. Sato, Special relativistic simulations of magnetically dominated jets in collapsing massive stars, Astrophys. J. **691**, 1360 (2009).
- [18] S. Scheidegger, R. Käppeli, S. C. Whitehouse, T. Fischer, and M. Liebendörfer, The influence of model parameters on the prediction of gravitational wave signals from stellar core collapse, Astron. Astrophys. **514**, A51 (2010).
- [19] P. Mösta, C. D. Ott, D. Radice, L. F. Roberts, E. Schnetter, and R. Haas, A large-scale dynamo and magnetoturbulence in rapidly rotating core-collapse supernovae, Nature (London) 528, 376 (2015).
- [20] H. Sawai and S. Yamada, The evolution and impacts of magnetorotational instability in magnetized core-collapse supernovae, Astrophys. J. 817, 153 (2016).
- [21] J. Matsumoto, T. Takiwaki, K. Kotake, Y. Asahina, and H. R. Takahashi, 2D numerical study for magnetic field

- dependence of neutrino-driven core-collapse supernova models, Mon. Not. R. Astron. Soc. **499**, 4174 (2020).
- [22] J. Matsumoto, Y. Asahina, T. Takiwaki, K. Kotake, and H. R. Takahashi, Magnetic support for neutrino-driven explosion of 3D non-rotating core-collapse supernova models, Mon. Not. R. Astron. Soc. **516**, 1752 (2022).
- [23] M. Bugli, J. Guilet, and M. Obergaulinger, Three-dimensional core-collapse supernovae with complex magnetic structures—I. Explosion dynamics, Mon. Not. R. Astron. Soc. 507, 443 (2021).
- [24] M. Bugli, J. Guilet, T. Foglizzo, and M. Obergaulinger, Three-dimensional core-collapse supernovae with complex magnetic structures—II. Rotational instabilities and multimessenger signatures, Mon. Not. R. Astron. Soc. 520, 5622 (2023).
- [25] M. Obergaulinger and M. Á. Aloy, Magnetorotational core collapse of possible GRB progenitors—I. Explosion mechanisms, Mon. Not. R. Astron. Soc. 492, 4613 (2020).
- [26] M. Obergaulinger and M. Á. Aloy, Magnetorotational core collapse of possible GRB progenitors—III. Threedimensional models, Mon. Not. R. Astron. Soc. 503, 4942 (2021).
- [27] M. Á. Aloy and M. Obergaulinger, Magnetorotational core collapse of possible GRB progenitors—II. Formation of protomagnetars and collapsars, Mon. Not. R. Astron. Soc. 500, 4365 (2021).
- [28] M. Obergaulinger and M. Á. Aloy, Magnetorotational core collapse of possible gamma-ray burst progenitors—IV. A wider range of progenitors, Mon. Not. R. Astron. Soc. **512**, 2489 (2022).
- [29] A. K. Alok, N. R. Singh Chundawat, and A. Mandal, Cosmic neutrino flux and spin flavor oscillations in intergalactic medium, Phys. Lett. B **839**, 137791 (2023).
- [30] J. Kopp, T. Opferkuch, and E. Wang, Magnetic moments of astrophysical neutrinos, arXiv:2212.11287.
- [31] S. Horiuchi and J. P. Kneller, What can be learned from a future supernova neutrino detection?, J. Phys. G **45**, 043002 (2018).
- [32] M.-R. Wu, Y.-Z. Qian, G. Martinez-Pinedo, T. Fischer, and L. Huther, Effects of neutrino oscillations on nucleosynthesis and neutrino signals for an 18 M supernova model, Phys. Rev. D **91**, 065016 (2015).
- [33] H. Sasaki, T. Takiwaki, S. Kawagoe, S. Horiuchi, and K. Ishidoshiro, Detectability of collective neutrino oscillation signatures in the supernova explosion of a $8.8M_{\odot}$ star, Phys. Rev. D **101**, 063027 (2020).
- [34] M. Zaizen, J. F. Cherry, T. Takiwaki, S. Horiuchi, K. Kotake, H. Umeda, and T. Yoshida, Neutrino halo effect on collective neutrino oscillation in iron core-collapse supernova model of a 9.6 M_{solar} star, J. Cosmol. Astropart. Phys. 06 (2020) 011.
- [35] M. Zaizen, S. Horiuchi, T. Takiwaki, K. Kotake, T. Yoshida, H. Umeda, and J. F. Cherry, Three-flavor collective neutrino conversions with multi-azimuthal-angle instability in an electron-capture supernova model, Phys. Rev. D 103, 063008 (2021).
- [36] C. Fröhlich, G. Martínez-Pinedo, M. Liebendörfer, F.-K. Thielemann, E. Bravo, W. R. Hix, K. Langanke, and N. T. Zinner, Neutrino-induced nucleosynthesis of A > 64 nuclei: The νp process, Phys. Rev. Lett. **96**, 142502 (2006).

- [37] H. Sasaki, T. Kajino, T. Takiwaki, T. Hayakawa, A. B. Balantekin, and Y. Pehlivan, Possible effects of collective neutrino oscillations in three-flavor multiangle simulations of supernova νp processes, Phys. Rev. D 96, 043013 (2017).
- [38] H. Sasaki, Y. Yamazaki, T. Kajino, M. Kusakabe, T. Hayakawa, M.-K. Cheoun, H. Ko, and G. J. Mathews, Impact of hypernova *νp*-process nucleosynthesis on the galactic chemical evolution of Mo and Ru, Astrophys. J. **924**, 29 (2022).
- [39] H. Sasaki, Y. Yamazaki, T. Kajino, and G. J. Mathews, Effects of Hoyle state de-excitation on νp-process nucleosynthesis and Galactic chemical evolution, arXiv:2307 .02785.
- [40] S. E. Woosley, D. H. Hartmann, R. D. Hoffman, and W. C. Haxton, The neutrino process, Astrophys. J. 356, 272 (1990).
- [41] T. Hayakawa, H. Ko, M.-K. Cheoun, M. Kusakabe, T. Kajino, M. D. Usang, S. Chiba, K. Nakamura, A. Tolstov, K. Nomoto, M.-a. Hashimoto, M. Ono, T. Kawano, and G. J. Mathews, Short-lived radioisotope ⁹⁸Tc synthesized by the supernova neutrino process, Phys. Rev. Lett. **121**, 102701 (2018).
- [42] H. Ko, D. Jang, M.-K. Cheoun, M. Kusakabe, H. Sasaki, X. Yao, T. Kajino, T. Hayakawa, M. Ono, T. Kawano, and G. J. Mathews, Comprehensive analysis of the neutrino process in core-collapsing supernovae, Astrophys. J. 937, 116 (2022).
- [43] M. C. Volpe, Neutrinos from dense: flavor mechanisms, theoretical approaches, observations, new directions, arXiv:2301.11814.
- [44] L. Wolfenstein, Neutrino oscillations in matter, Phys. Rev. D 17, 2369 (1978).
- [45] S. P. Mikheyev and A. Yu. Smirnov, Resonance amplification of oscillations in matter and spectroscopy of solar neutrinos, Sov. J. Nucl. Phys. 42, 913 (1985).
- [46] J. T. Pantaleone, Neutrino oscillations at high densities, Phys. Lett. B **287**, 128 (1992).
- [47] J. T. Pantaleone, Dirac neutrinos in dense matter, Phys. Rev. D 46, 510 (1992).
- [48] G. Sigl and G. Raffelt, General kinetic description of relativistic mixed neutrinos, Nucl. Phys. B406, 423 (1993)
- [49] B. H. J. McKellar and M. J. Thomson, Oscillating doublet neutrinos in the early universe, Phys. Rev. D **49**, 2710 (1994).
- [50] S. Yamada, Boltzmann equations for neutrinos with flavor mixings, Phys. Rev. D 62, 093026 (2000).
- [51] A. B. Balantekin and Y. Pehlivan, Neutrino-neutrino interactions and flavor mixing in dense matter, J. Phys. G 34, 47 (2007).
- [52] Y. Pehlivan, A. B. Balantekin, T. Kajino, and T. Yoshida, Invariants of collective neutrino oscillations, Phys. Rev. D 84, 065008 (2011).
- [53] A. Vlasenko, G. M. Fuller, and V. Cirigliano, Neutrino quantum kinetics, Phys. Rev. D 89, 105004 (2014).
- [54] C. Volpe, D. Väänänen, and C. Espinoza, Extended evolution equations for neutrino propagation in astrophysical and cosmological environments, Phys. Rev. D 87, 113010 (2013).

- [55] D. N. Blaschke and V. Cirigliano, Neutrino quantum kinetic equations: The collision term, Phys. Rev. D 94, 033009 (2016).
- [56] S. Richers and M. Sen, Fast flavor transformations, arXiv:2207.03561.
- [57] A. V. Patwardhan, M. J. Cervia, E. Rrapaj, P. Siwach, and A. B. Balantekin, Many-body collective neutrino oscillations: Recent developments, arXiv:2301.00342.
- [58] A. B. Balantekin, M. J. Cervia, A. V. Patwardhan, E. Rrapaj, and P. Siwach, Quantum information and quantum simulation of neutrino physics, Eur. Phys. J. A 59, 186 (2023).
- [59] E. K. Akhmedov and Z. G. Berezhiani, Implications of Majorana neutrino transition magnetic moments for neutrino signals from supernovae, Nucl. Phys. B373, 479 (1992).
- [60] E. K. Akhmedov, S. T. Petcov, and A. Y. Smirnov, Neutrinos with mixing in twisting magnetic fields, Phys. Rev. D 48, 2167 (1993).
- [61] T. Totani and K. Sato, Resonant spin flavor conversion of supernova neutrinos and deformation of the anti-electronneutrino spectrum, Phys. Rev. D 54, 5975 (1996).
- [62] H. Nunokawa, Y. Z. Qian, and G. M. Fuller, Resonant neutrino spin flavor precession and supernova nucleosynthesis and dynamics, Phys. Rev. D 55, 3265 (1997).
- [63] S. Ando and K. Sato, Three generation study of neutrino spin flavor conversion in supernova and implication for neutrino magnetic moment, Phys. Rev. D 67, 023004 (2003).
- [64] S. Ando and K. Sato, Resonant spin flavor conversion of supernova neutrinos: Dependence on presupernova models and future prospects, Phys. Rev. D 68, 023003 (2003).
- [65] S. Ando and K. Sato, A comprehensive study of neutrino spin flavor conversion in supernovae and the neutrino mass hierarchy, J. Cosmol. Astropart. Phys. 10 (2003) 001.
- [66] E. K. Akhmedov and T. Fukuyama, Supernova prompt neutronization neutrinos and neutrino magnetic moments, J. Cosmol. Astropart. Phys. 12 (2003) 007.
- [67] A. Ahriche and J. Mimouni, Supernova neutrino spectrum with matter and spin flavor precession effects, J. Cosmol. Astropart. Phys. 11 (2003) 004.
- [68] T. Yoshida, A. Takamura, K. Kimura, H. Yokomakura, S. Kawagoe, and T. Kajino, Resonant spin-flavor conversion of supernova neutrinos: Dependence on electron mole fraction, Phys. Rev. D 80, 125032 (2009).
- [69] T. Bulmus and Y. Pehlivan, Spin-flavor precession phase effects in supernova, arXiv:2208.06926.
- [70] S. Jana, Y. P. Porto-Silva, and M. Sen, Exploiting a future galactic supernova to probe neutrino magnetic moments, J. Cosmol. Astropart. Phys. 09 (2022) 079.
- [71] S. Jana and Y. Porto, New resonances of supernova neutrinos in twisting magnetic fields, arXiv:2303.13572.
- [72] A. de Gouvea and S. Shalgar, Effect of transition magnetic moments on collective supernova neutrino oscillations, J. Cosmol. Astropart. Phys. 10 (2012) 027.
- [73] A. de Gouvea and S. Shalgar, Transition magnetic moments and collective neutrino oscillations: Three-flavor effects and detectability, J. Cosmol. Astropart. Phys. 04 (2013) 018.

- [74] S. Abbar, Collective oscillations of Majorana neutrinos in strong magnetic fields and self-induced flavor equilibrium, Phys. Rev. D 101, 103032 (2020).
- [75] H. Sasaki and T. Takiwaki, Neutrino-antineutrino oscillations induced by strong magnetic fields in dense matter, Phys. Rev. D 104, 023018 (2021).
- [76] B. Dasgupta and A. Dighe, Collective three-flavor oscillations of supernova neutrinos, Phys. Rev. D 77, 113002 (2008).
- [77] H. Duan, G. M. Fuller, and Y.-Z. Qian, Collective neutrino oscillations, Annu. Rev. Nucl. Part. Sci. 60, 569 (2010).
- [78] I. Tamborra and S. Shalgar, New developments in flavor evolution of a dense neutrino gas, Annu. Rev. Nucl. Part. Sci. 71, 165 (2021).
- [79] F. Capozzi and N. Saviano, Neutrino flavor conversions in high-density astrophysical and cosmological environments, Universe **8**, 94 (2022).
- [80] H. Nagakura and M. Zaizen, Time-dependent and quasisteady features of fast neutrino-flavor conversion, Phys. Rev. Lett. **129**, 261101 (2022).